Journal of Biomedical Optics

SPIEDigitalLibrary.org/jbo

Assessment of thermal effects of interstitial laser phototherapy on mammary tumors using proton resonance frequency method

Kelvin Le
Xiaosong Li
Daniel Figueroa
Rheal A. Towner
Philippe Garteiser
Debra Saunders
Nataliya Smith
Hong Liu
Tomas Hode
Robert E. Nordquist
Wei R. Chen

SPIE

Assessment of thermal effects of interstitial laser phototherapy on mammary tumors using proton resonance frequency method

Kelvin Le,[a,*] Xiaosong Li,[a,b,c,*] Daniel Figueroa,[a] Rheal A. Towner,[d] Philippe Garteiser,[d] Debra Saunders,[d] Nataliya Smith,[d] Hong Liu,[e] Tomas Hode,[f] Robert E. Nordquist,[f] and Wei R. Chen[a]
[a]University of Central Oklahoma, Department of Engineering and Physics, Edmond, Oklahoma 73034
[b]The First Affiliated Hospital of Chinese PLA General Hospital, The Second Department of Oncology, Beijing 100048, China
[c]Chinese PLA General Hospital, Department of Laser Medicine, Beijing 100853, China
[d]Oklahoma Medical Research Foundation, Advanced Magnetic Resonance Center, 825 NE 13th Street, Oklahoma City, Oklahoma 73104
[e]University of Oklahoma, Center for Bioengineering and School of Electrical and Computer Engineering, Norman, Oklahoma 73019
[f]ImmunoPhotonics Inc., Columbia, Missouri 65211

Abstract. Laser immunotherapy (LIT) uses a synergistic approach to treat cancer systemically through local laser irradiation and immunological stimulation. Currently, LIT utilizes dye-assisted noninvasive laser irradiation to achieve selective photothermal interaction. However, LIT faces difficulties treating deeper tumors or tumors with heavily pigmented overlying skin. To circumvent these barriers, we use interstitial laser irradiation to induce the desired photothermal effects. The purpose of this study is to analyze the thermal effects of interstitial irradiation using proton resonance frequency (PRF). An 805-nm near-infrared laser with an interstitial cylindrical diffuser was used to treat rat mammary tumors. Different power settings (1.0, 1.25, and 1.5 W) were applied with an irradiation duration of 10 min. The temperature distributions of the treated tumors were measured by a 7 T magnetic resonance imager using PRF. We found that temperature distributions in tissue depended on both laser power and time settings, and that variance in tissue composition has a major influence in temperature elevation. The temperature elevations measured during interstitial laser irradiation by PRF and thermocouple were consistent, with some variations due to tissue composition and the positioning of the thermocouple's needle probes. Our results indicated that, for a tissue irradiation of 10 min, the elevation of rat tumor temperature ranged from 8 to 11°C for 1 W and 8 to 15°C for 1.5 W. This is the first time a 7 T magnetic resonance imager has been used to monitor interstitial laser irradiation via PRF. Our work provides a basic understanding of the photothermal interaction needed to control the thermal damage inside a tumor using interstitial laser treatment. Our work may lead to an optimal protocol for future cancer treatment using interstitial phototherapy in conjunction with immunotherapy. [DOI: 10.1117/1.3659200]

Keywords: proton resonance frequency; rat tumor; interstitial laser irradiation; cylindrical diffuser; tissue temperature elevation.

Paper 11371RR received Jul. 13, 2011; revised manuscript received Oct. 18, 2011; accepted for publication Oct. 19, 2011; published online Dec. 5, 2011.

1 Introduction

Late-stage, metastatic cancers pose a great challenge in cancer treatment. Commonly used treatment modalities, such as surgery, chemotherapy, and radiation, all have limited effects on metastatic cancers. In its inchoate stages, immunotherapy has been considered a promising treatment modality for metastatic cancers. Many new strategies have been proposed, including cytokine therapy,[1,2] dendritic cell-based vaccines,[3,4] and immune-activating antibodies,[5,6] which have begun to be used in clinical studies, either alone or in various combinations with other therapies. However, so far immunotherapy only has made limited progress in cancer treatment.[7]

A systemic, synergistic approach with an immunological root is a more attractive option for treating metastatic cancers. Laser immunotherapy (LIT), which combines both phototherapy and immunotherapy, is a noninvasive approach that targets the host's immune system for long-term tumor suppression.[8] This combination synthesizes the local and systemic successes of phototherapy and immunotherapy, respectively. LIT combines a laser for tumor irradiation, a light absorbing dye for enhanced selectivity, and a unique biocompatible immunoadjuvant glycated chitosan for immunological stimulation.[9–13] The laser light causes target temperature to rise, killing cancer cells while releasing antigens. The pinnacle of LIT is not local tumor destruction itself, but rather the systemic immunological effect that it triggers following local treatment. Although still in its developmental stage, laser immunotherapy has already shown significant clinical success for late-stage melanoma and breast cancer patients.[14–16]

[*]Authors contributed equally to this work.

Address all correspondence to: Wei Chen, University of Central Oklahoma, Department of Engineering and Physics, 221 G Howell Hall, Edmond, Oklahoma 73034. Tel: 405 974-5198; Fax: 405 974-3812; E-mail: wchen@uco.edu.

1083-3668/2011/16(12)/128001/10/$25.00

Photothermal interaction is an integral part of LIT. Selective photothermal tumor destruction was proposed using *in situ* administration of indocyanine green.[17–19] It has long been established that cancer cells are more sensitive to temperature elevation than normal cells. Thermal injury to tumor cells is also considered to be a precursor for immune activation by increasing the temperature in target tumor. Some of the by-products of the thermal interaction include tumor-associated antigens, thermally induced heat shock proteins (HSPs), and a number of self-antigens.[20–22] Antigen presenting cells, particularly dendritic cells, can capture these antigens, migrate to lymph nodes, and present the antigens to T cells to induce antitumor immune responses.[23–25] Specifically, it is known that the thermal treatment of primary tumors can induce the release of unique tumor antigenic peptides that are bound to HSPs.[26–29] However, high levels of laser irradiation can lead to total tissue destruction and may hamper host immune response in the process. Therefore, laser-tissue interaction induced by LIT must be administered with proper guidance.

Previously, laser immunotherapy has mainly focused on noninvasive light delivery using dye-enhanced selective thermal interaction.[17–19] The procedure requires a laser diffuser to be held over the treatment site with an *in situ* light absorbing dye. However, in nonideal cases where the skin surface is pigmented or when treatment involves deep subcutaneous tumors, the results can be less effective due to the limitation of light penetration in tissue. Pigmented skin and the normal tissue between the treatment surface and the deep tumor absorb the most incident light energy, limiting photothermal interaction in target tissue. Increasing the irradiation power will cause more damage to the healthy tissue, minimizing the therapeutic effects. In the interest of expanding LIT beyond surface treatments, we began to develop interstitial laser immunotherapy (ILIT). When the laser light is directed into the target tissue through an interstitial fiber, surface damage can be avoided and the deep tumor can be reached. However, appropriate thermal interaction is still crucial in order to achieve a long-term, systemic effect for cancer treatment. Hence, advances in this field require effective and reliable temperature determination.

Most conventional temperature measurement methods, such as thermocouple and infrared imaging, involve interstitial intervention and can only acquire the temperature at specific locations. Measurement using thermocouples requires the positioning of needle probes in tissue, making precise spatial determination extremely difficult. A thermal camera usually provides only the temperature distribution on the surface. Furthermore, during laser phototherapy, temperature measurements using these conventional methods interfere with the treatment procedures. These obstacles can be overcome by using magnetic resonance thermometry (MRT). Temperature measurements based on water proton resonance frequency (PRF) have been widely used. PRF exploits the temperature dependency of the water proton's chemical shift to measure temperature.[30–36] More importantly, MRT using PRF can provide three-dimensional (3D) temperature profiles inside and outside the target tissue. This method can be used to measure tumor temperature during laser irradiation with minimal interference. It could become an integral part of an imaging-guided treatment modality when combined with laser immunotherapy.

PRF is ideal for measuring target tissue temperature during interstitial laser irradiation. In the present study, we used PRF to assess thermal effects during the treatment of animal tumors with an infrared laser. An interstitial fiber with an active cylindrical tip was used. Temperature distributions inside tumors were determined using PRF and thermocouples during interstitial laser irradiation. Our goal is to test the feasibility of the PRF method for temperature determination during interstitial laser irradiation, and to use the results of current and future studies to develop an interstitial laser immunotherapy protocol for clinical applications.

2 Methods and Procedures

2.1 *Interstitial Laser Irradiation*

An 805-nm diode laser (Delta-30, AngioDynamics, Queensbury, New York) was used to deliver near-infrared light for all tissues. Continuous laser power was delivered through a 7-m optical fiber with an active cylindrical tip (Pioneer Optics, Windsor Locks, Connecticut). Active tips of 0.5 and 1.0 cm were used. To verify the procedures, bovine liver was used for temperature measurements during laser irradiation with the 1.0-cm active tip, which allowed a more comprehensive temperature assessment (more image slices along the active tip) and an easier slice selection process. In the rat experiments the 0.5-cm active tip was used due to the physical constraint of the small tumor size. Figure 1(a) shows the configurations of the long and short active tips in tissue. Prior to all laser irradiation, actual power outputs

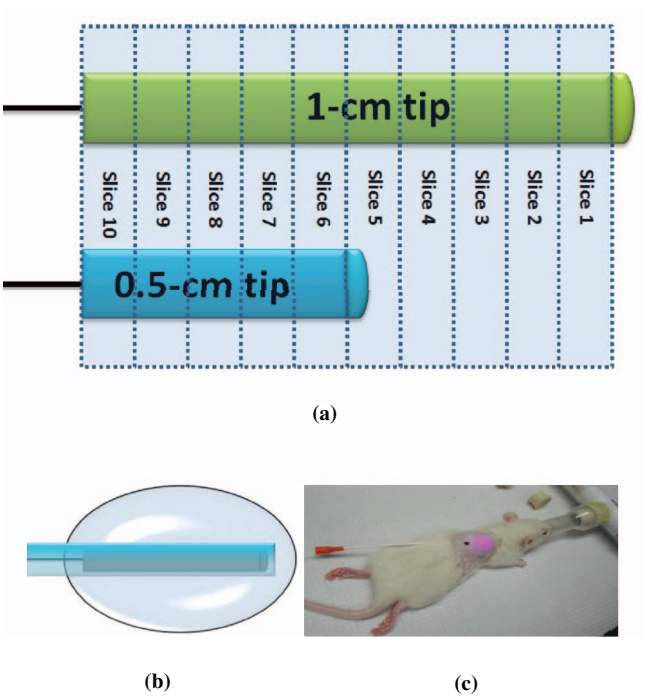

Fig. 1 (a) Schematics of the configuration for 1- and 0.5-cm active tips in tissue and the MRI slice selection. Ten 1-mm transverse slices were selected along the laser fiber (*z*-axis) for image acquisition. The 1 and 0.5-cm active tips are used for the *ex vivo* bovine liver and *in vivo* rat experiments, respectively. (b) Schematic of the active tip placed inside a rat tumor, protected by a sheath. (c) Irradiation of a rat tumor using an interstitial fiber.

for various power settings were determined using a spherical power meter (Ophir-Spiricon, Logan, Utah).

2.2 *Tumor Preparation*

Wistar Furth female rats were injected with 10^5 DMBA-4 metastatic mammary tumor cells on their upper backs. Interstitial laser irradiation was applied when the tumors grew to a size of 1 to 1.5 cm in diameter. For the PRF experiment, the rat was allowed to rest in a prone position in an acrylic tube placed inside the bore of the magnetic resonance imager. In addition, gating sensors were attached to the rat's body. A dedicated computer in the control room was used to monitor the rat's respiration using a respiration pillow and SAM PC gating software (SAI Instruments, Manchester, England). During treatment, anesthesia (1.5% 2% Isofluorane, 800 to 1000 ml/min O_2) was administered to keep a stable respiration rate (~35 breaths/min).

2.3 *Experimental Setup for PRF*

For bovine liver, the active tip was inserted directly into a preselected location. For animal tumors, a small needle (20 gauge) was used to make the preliminary incision into the tumor, followed by a larger needle (14 gauge). The 0.5-cm cylindrical active tip was inserted into the center of the tumor guided by the preinserted 14 gauge needle. A transparent plastic sheath was used to protect the laser fiber. The position of the fiber and the rat experiment setup are shown in Figs. 1(b) and 1(c). The laser power and irradiation duration were as follows: 1 W for 10 min, 1.25 W for 10 min, or 1.5 W for 10 min.

2.4 *Experimental Setup for Thermocouple Measurements*

For the thermocouple measurement, each rat was placed in a prone position during laser irradiation. Experiments were conducted using the 0.5-cm active tip with a laser power of 1 or 1.5 W for 10 min. Before the experiment, the thermocouples were calibrated on InstruNET software (Omega Engineering, Stamford, Connecticut) using freezing and boiling baths at 0°C and 98°C, respectively. To acquire the temperature data, the thermocouple needles were first sterilized and then inserted into the target tissue at varying distances from the center of the cylindrical active tip. Two thermocouple needle probes were placed 2 and 5 mm away from the laser fiber.

2.5 *Calibrations and Verification*

To calibrate the equipment and to verify the PRF method, *ex vivo* bovine liver tissue was cooled to 0°C overnight in an ice water bath and then brought back to 4°C before MRI imaging. Different points in the tissue were chosen for photothermal assessment with respect to the active tip. PRF was used to measure bovine liver tissue temperature profiles during a 10 min laser irradiation with 1.5 W using the 1-cm active tip. A similar experiment was performed on bovine liver tissue with temperature measurement using thermocouples with needle probes inserted 2, 3, and 5 mm from the active tip.

2.6 *PRF Method*

PRF temperature dependency was first investigated by Hindman.[33] However, the application of PRF for temperature mapping was first proposed by Ishihara et al.[37] The PRF temperature mapping theory describes how the relationship between the external magnetic field and the local magnetic field are linked by the temperature dependent shielding factor. As described by Hindman and Ishihara et al., the shielding factor of nuclei, which expresses the relationship between the external and local magnetic fields, is sensitive to temperature. Hence, in PRF experiments the temperature is measured via changes in signal phase which result from variations in the shielding constant, according to:

$$\Delta T = \frac{\Delta\phi}{\gamma B_0 \alpha T E}, \tag{1}$$

where ΔT is the change in temperature (°C), $\Delta\phi$ is the change in phase, γ is the gyromagnetic ratio (MHz/T), B_0 is the magnetic field (T), α is the thermal coefficient ($^\circ C^{-1}$), and TE is the echo time (s).

PRF was used to evaluate temperature profiles during laser irradiation. All experiments were performed using a 7 T Bruker 730 USR horizontal-bore MR imaging system equipped with a 15-cm diameter quadrature volume coil and controlled by Para Vision 5.0 Software (Bruker BioSpin MRI GmbH, Germany). A fast low angle shot (FLASH) gradient-echo pulse sequence was used for optimal temporal resolution and reliability.[38–40] The echo time (TE) and repetition time were set at 4 and 200 ms, respectively. Ten 1-mm slices were partitioned along the length of the active cylindrical tip, as shown in Fig. 1(a). For the best temporal resolution, the number of averages was set to 1. The flip angle was set at 30 deg based on the temporal resolution priority. To minimize motion artifacts in the rat experiments, the scans were gated to the respiration of the animal. Consequently, the temporal resolution can only be approximated by an average with uncertainty depending on the steady state of the rat's respiration. The data acquisitions were obtained during the longest steady state, which was the inhalation period. The approximate temporal resolution was 1 min/cycle. The actual average temporal resolution was determined by recording the final time elapsed and dividing it by the number of cycles. An abnormal breathing rate could prolong scans and affect the overall reliability of the temporal resolution measurement. The field of view (FOV) was set to 50×50 mm, with 128×128 pixels, providing a spatial resolution of 2.56 pixels/mm or 2 mm for every 5 pixels. The system was configured to acquire between 20 to 25 cycles with an estimated time of 20 to 25 min. MRI imaging was performed 5 min before and 5 min after laser irradiation. Prior to each data acquisition, high-resolution (256×256) magnitude scans were acquired to locate the laser fiber.

A similar MRI configuration was used for the bovine liver experiment. Ten 1-mm slices were partitioned along the length of the 1-cm active cylindrical tip, as shown in Fig. 1(a). The FOV was set to 60×23 mm, providing a spatial resolution of 2.13 and 5.57 pixels/mm along the horizontal and vertical axes, respectively. The total acquisition cycle was 44, with a total time of 18 min. Without gating, the temporal resolution for the liver experiment was 25.7 s/cycle.

2.7 *Image Processing*

Using the real (Re_n) and imaginary (Im_n) parts of the acquired imaging data, the phase difference ($\Delta\phi$) between the phase at frame number n (ϕ_n) and the initial phase (ϕ_o) was calculated using the following equation,

$$\Delta\phi = \phi_n - \phi_o = \text{ArcTan}\left(\frac{Re_n\, Im_o - Re_o\, Im_n}{Re_o\, Re_n + Im_o\, Im_n}\right). \quad (2)$$

Subsequently, the temperature elevation was obtained from the phase-temperature relation given in Eq. (1). Temperature maps were calculated using MATLAB 2008 version 7.6 (The MathWorks Inc, Boston, Massachusetts). A 9-pixel region of interest (ROI) was sampled and averaged over time in close proximity to the laser fiber (1, 3, 5, or 10 mm). The laser fiber location was determined using the magnitude map. However, these distances are under the physical constraint of the target tissue.

3 Results

3.1 *Bovine Liver Temperature Profiles*

To obtain temperature maps in bovine liver, 10 transverse MR thermographic isoplots of tissue temperature were acquired along the 1-cm active tip. Two-dimensional (2D) temperature distributions in the three middle slices of the liver tissue are given in Fig. 2(a). Taking advantage of the 2D temperature profile, temperature data points on the transverse cross-section of the fifth slice along the x and y directions were extracted and analyzed, as shown in Figs. 2(b) and 2(c). Sharp temperature gradients were observed in close proximity to the active tip (10°C over just 1 mm of displacement). To test the reliability of the PRF measurement, thermocouples were used in a separate experiment. Choosing a specific transverse plane, temperature elevations at different locations measured by the two different methods were compared in Figs. 3(a) and 3(b).

Due to the difficulties in determining the exact location of the thermocouple in tissue, the two temperature profiles in Figs. 3(a) and 3(b) do not match exactly. However, the range and the trend of the temperature elevation indicate that PRF is a reliable method to allow a comprehensive assessment of the nuanced spatial temperature elevation throughout the target tissue.

3.2 *Temperature Measurement During Laser Treatment of Rat Tumors Using PRF*

Rat tumors were treated with interstitial laser irradiation under a power of 1.25 W and a duration of 10 min. The active tip entry point can be clearly seen in the corresponding magnitude profile, as shown in Fig. 4(a), left panel. The temperature increases within a specific transverse plane are also shown in Fig. 4(a), right panel. The peak temperature elevation, 1 mm away from the active tip, was about 25°C.

A set of images, representing various cross-sections along the active tip and providing a 3D view of the temperature distribution inside the tumor, is shown in Fig. 4(b). The temperature reached its peak near the center of the active tip (slice 7). A closer look at points 1 and 3 mm from the active tip of the fifth slice revealed that the temperature elevation fluctuates over time, as shown in

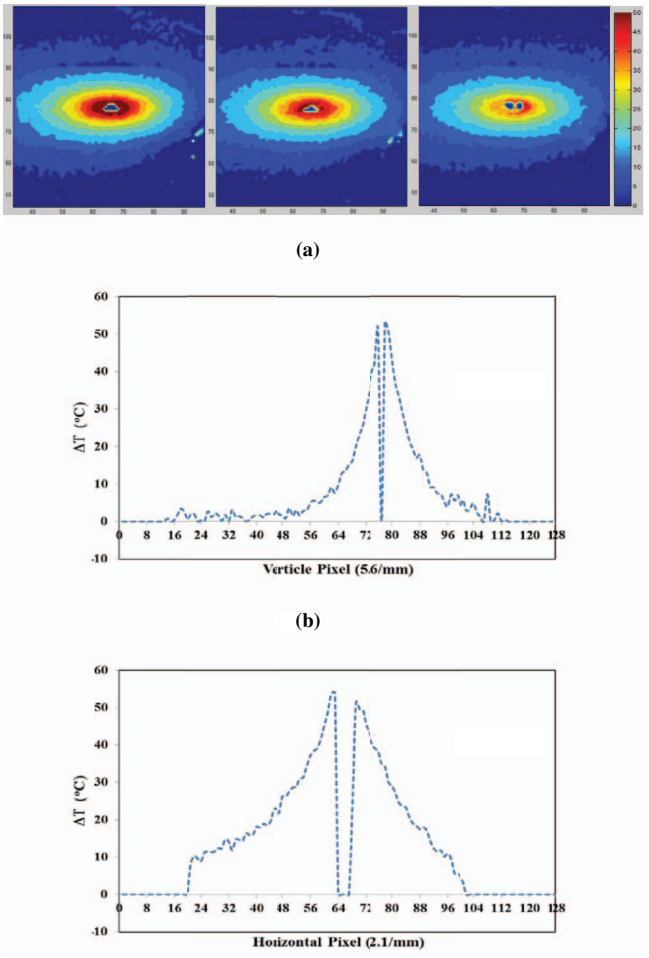

Fig. 2 Bovine liver 1.5 W PRF spatial assessment. (a) Two-dimensional temperature distributions in liver tissue immediately after interstitial laser irradiation (1.5 W for 10 min) at different locations: Slice 6 (left panel), slice 5 (middle panel), and slice 4 (right panel). See Fig. 1(a) for the selection of slices with the 1-cm active tip. Liver tissue temperature elevations along the x-axis (b) and y-axis (c) on the transverse plane of the fifth slice, immediately after the interstitial laser irradiation (1.5 W for 10 min). A large temperature gradient is observed in close vicinity to the active tip.

Fig. 5. The rate of temperature elevation reaching a steady state was lower than that of the bovine liver.

MR thermographic isoplots of tissue temperature were acquired for a rat tumor before and after irradiation with a laser power of 1.0 W and duration of 10 min, as shown in Fig. 6(a). The temperature elevation reached 7°C and 8°C with a distance of 3 and 1 mm away from the active tip, respectively, as shown in Fig. 6(b). The temperature elevation differed only by 2°C for a 2-mm displacement. This temperature gradient is smaller compared to that of higher laser powers.

Likewise, MR thermographic isoplots of tissue temperature were acquired for a rat tumor before and after irradiation with a laser power of 1.5 W and a duration of 10 min, as shown in Figs. 6(c) and 6(d). The temperature elevation reached 8°C and 17°C at 3 mm and 1 mm away from the active tip, respectively, as shown in Fig. 6(d). With the power increased, the thermal damage due to temperature elevation also increased. These

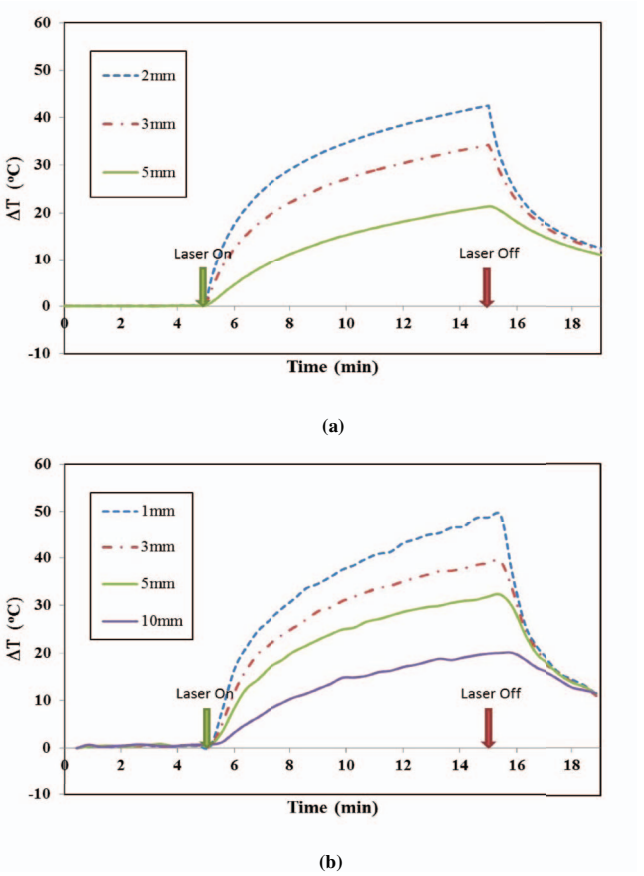

Fig. 3 Bovine liver 1.5 W thermocouple and PRF temporal assessments. Liver tissue temperature elevations at different locations during interstitial laser irradiation (1.5 W for 10 min), measured by thermocouple (a) and PRF (b). The transverse plane of these measurements was the fifth slice. See Fig. 1(a) for the selection of slices with the 1-cm active tip. The transverse distance from the active tip ranges from 2 to 5 mm for thermocouple and 1 to 10 mm for PRF.

relatively larger temperature differences may allow a wider range of immunological responses.

3.3 *Temperature Measurement During Laser Treatment of Rat Tumors Using Thermocouples*

Temperature increases in a rat tumor were also measured at distances of 2 and 5 mm from the active tip using thermocouples to validate the results of PRF. For a tissue irradiation of 10 min, the elevation of a rat tumor temperature ranged from 8°C to 11°C for 1 W and 8°C to 15°C for 1.5 W, as shown in Fig. 7.

4 Discussion

4.1 *Calibrations and Observations of Phase Drift*

One of the advantages of PRF is its near independence from tissue composition. It has been reported by Bruno et al. that the thermal coefficient of swine liver, kidney, and muscle is approximately 0.01 ppm/°C.[32] This is an assumption we used for both the bovine liver and the rat tumor in the PRF measurement of tissue temperatures.

It has been documented that chemical drift observed in an MR system is due to instability of the magnetic field,[41,42] and such an artifact is amplified over time.[43] Nevertheless, accurate and reliable temperature profiles can be extracted in the 20 to 30 min range depending on factors such as TE and tissue susceptibility.[36] As reported by Olsrud et al., during the first 30 min of their experiments using a 1.5 T MRI scanner, the corresponding temperature due to phase drift measured was approximately 1°C. Following this argument, for a stronger magnetic field of 7 T, the temperature corresponding to the phase drift should be even less significant (<1°C). Efforts to cope with these drifts are still being investigated. Instances of such endeavors are preacquisition K-space correction and post-acquisition linear regression.[44] These methods suppress the misalignment of the echo in the K-space, which according to Grimault et al.[43] contributes significantly to time-dependent background phase variations.

4.2 *Motion Artifacts*

An unstable respiration rate and the treatment location (near the heart or stomach) are the main contributing factors to motion artifacts in PRF measurement. Even though the acquisition is gated, motion artifacts are sometimes unavoidable, as seen in Fig. 5. Tumors near the stomach and heart are also susceptible to motion artifacts. In addition, gating interference due to the rat's erratic respiration can distort the temporal resolution. To enhance image clarity, a masking magnitude filter was implemented in our experiment.

4.3 *Phase Wrapping in PRF Method*

Phase wrapping was due to phase overlaps. This issue was resolved with a simple MATLAB code using a threshold setting, as shown in the Appendix. The code took the original 3D temperature data set, and then applied the unwrapping threshold to each individual pixel to calculate the unwrapped temperature. This unwrapping method is based on the simple assumption that the temperature elevation cannot be less than a certain negative value, since we are applying heat to the tissue. Thus, whenever the condition is met, the data will be offset by adding twice the maximum temperature increase. The result from this method is then processed as a normal data set.

4.4 *Temperature Measurement Using Bovine Liver Tissue*

High spatial and temporal resolutions are attained with FLASH image sequencing for *ex vivo* experiments using a bovine liver tissue. The temperature is uniformly distributed in an elliptical fashion, as shown in Fig. 2(a), which is consistent with the results reported by Olsrud et al.[36] The results from PRF and thermocouple measurements for the liver tissue were within a reasonable range for comparison. For example, at positions of 2, 3, and 5 mm, changes of 43°C, 33°C, 20°C were observed, respectively, using thermocouples, as shown in Fig. 3(a). At positions of 1, 3, and 5 mm away from the active tip, temperature changes of 50°C, 40°C, and 35°C were observed, respectively, using PRF, as shown in Fig. 3(b). The differences between the results are partly attributed to the thermocouple positioning error.

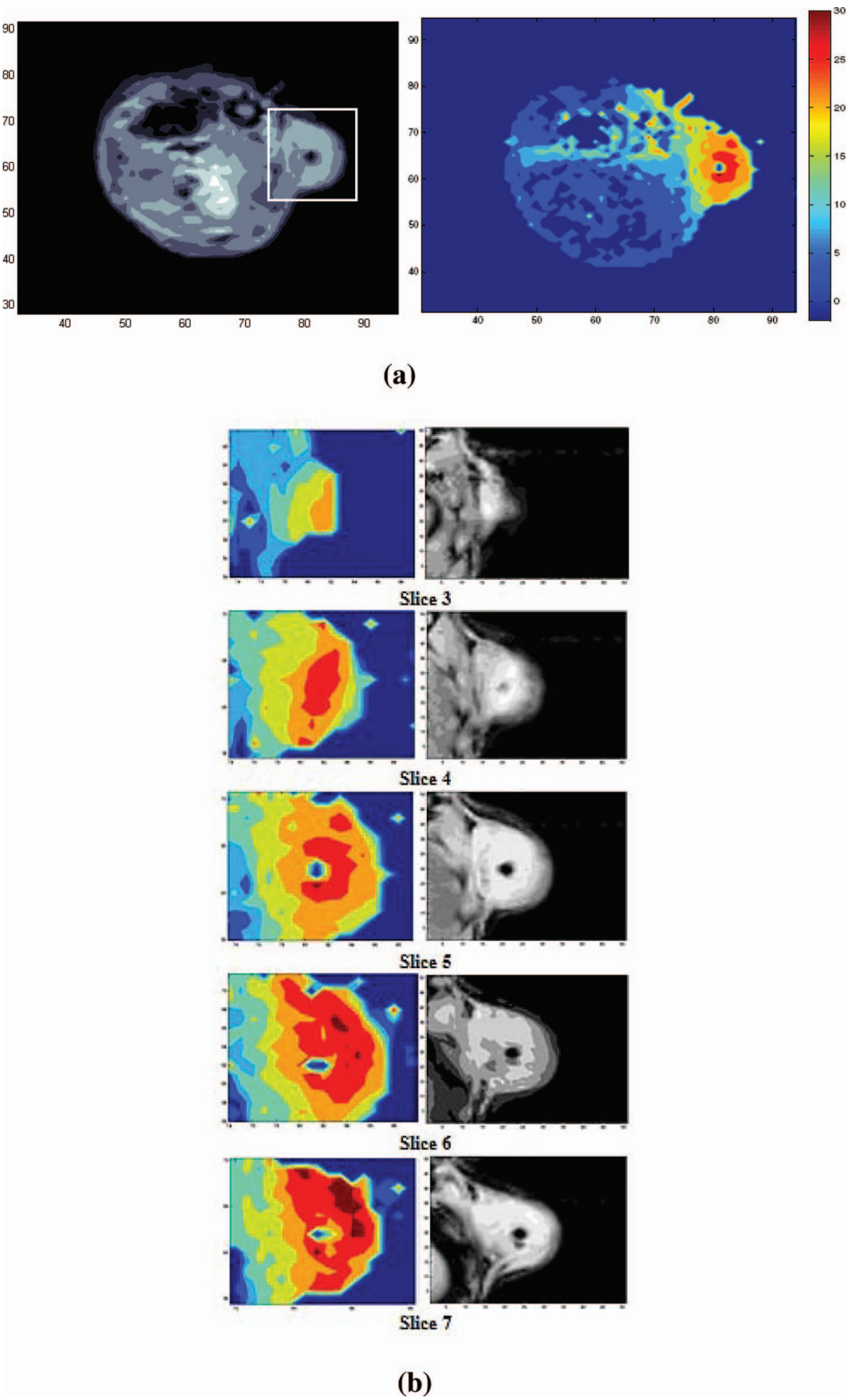

Fig. 4 Rat 1.25 W PRF spatial assessment. (a) Two-dimensional map of temperature elevation in a rat immediately after interstitial laser treatment (1.25 W for 10 min). A magnitude image (left panel) was used to help locate the active tip's entry point for alignment purposes. See Fig. 1(a) for the selection of slices with the 0.5-cm active tip. The corresponding temperature increases on the fifth slice (right panel), indicated that the temperature elevation peaked at 25°C at a location 1 mm away from the active tip. (b) Two-dimensional temperature distribution of a rat tumor using five different transverse slices, immediately after interstitial laser irradiation (1.25 W and 10 min). The end of the active tip can be seen in the fifth slice. Higher temperature elevations are correlated with increasing slice number, which is consistent with our liver results. Each temperature distribution map (left column) is shown with its corresponding magnitude image (right column).

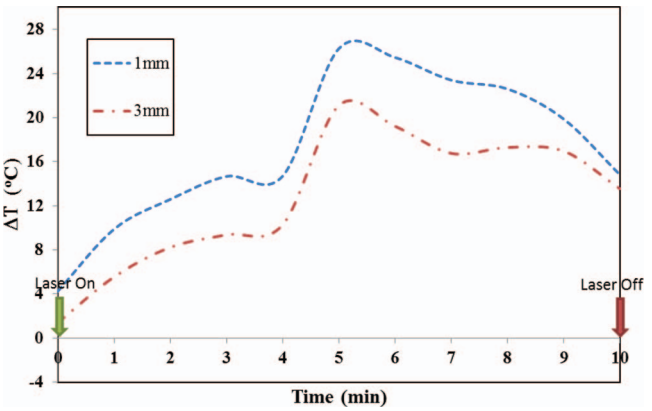

Fig. 5 Rat 1.25 W PRF temporal assessment. Temperature elevation in a rat tumor during interstitial laser treatment measured at positions 1 and 3 mm from the active tip using the fifth slice. See Fig. 1(a) for the selection of slices with the 0.5-cm active tip. The rate of temperature elevation reaching a steady state is slower compared with that of the liver tissue, due to different tissue thermal insulation factors such as fat content and skin thickness. The data fluctuations are partly due to the distorted temporal resolution of the measurement caused by the slow respiration rate of the rat.

4.5 *Thermocouple Measurement*

The rat thermocouple experiments yielded reasonable results, which helped guide our evaluation of the PRF results. The results are comparable to that of the PRF experiments, as shown in Figs. 6(b), 6(d), and 7. The differences observed are largely attributed to tissue composition and thermocouple positioning.

Interestingly, one may observe the large difference in thermal response between the liver and rat tumor tissues. Indeed, a similar power of 1.5 W was applied to liver and rat tumor tissues [Figs. 3(b) and 6(d)]. However, as the data indicated, the liver tissue temperature increase was roughly three-fold higher in comparison with that of the rat tumor. This is not completely unexpected, however, partly for the following reasons. First, these are two different types of tissue. The liver tissue is relatively homogeneous and heavily pigmented compared to the rat tumor tissue. Therefore, we can reasonably expect different photothermal properties such as conduction and scattering. Second, these experiments were conducted under different natural conditions. The *ex vivo* liver allowed more control but lacked the blood-perfusion present in the *in vivo* rat tumor experiment. In the *in vivo* experiments, the tissue is constantly perfused by fresh blood, and heated blood is constantly evacuated out of the irradiated region by cardiac-induced flow. Thus temperature elevation in the rat tumor occurred at a lower rate than what is shown in Fig. 3 for liver tissue.

4.6 *Thermal Effects of Interstitial Laser Irradiation*

Numerous PRF thermal profiles made it possible to assess the photothermal effect for various slices along the active tip. With this method, we were able to detect the uneven distribution of laser power along the active tip, as shown in Figs. 2(b) and 2(c). Abnormal temperature distributions were also observed; they were mainly due to diversity in tissue composition including lipids, necrosis, and fluids. These factors may also affect the rate

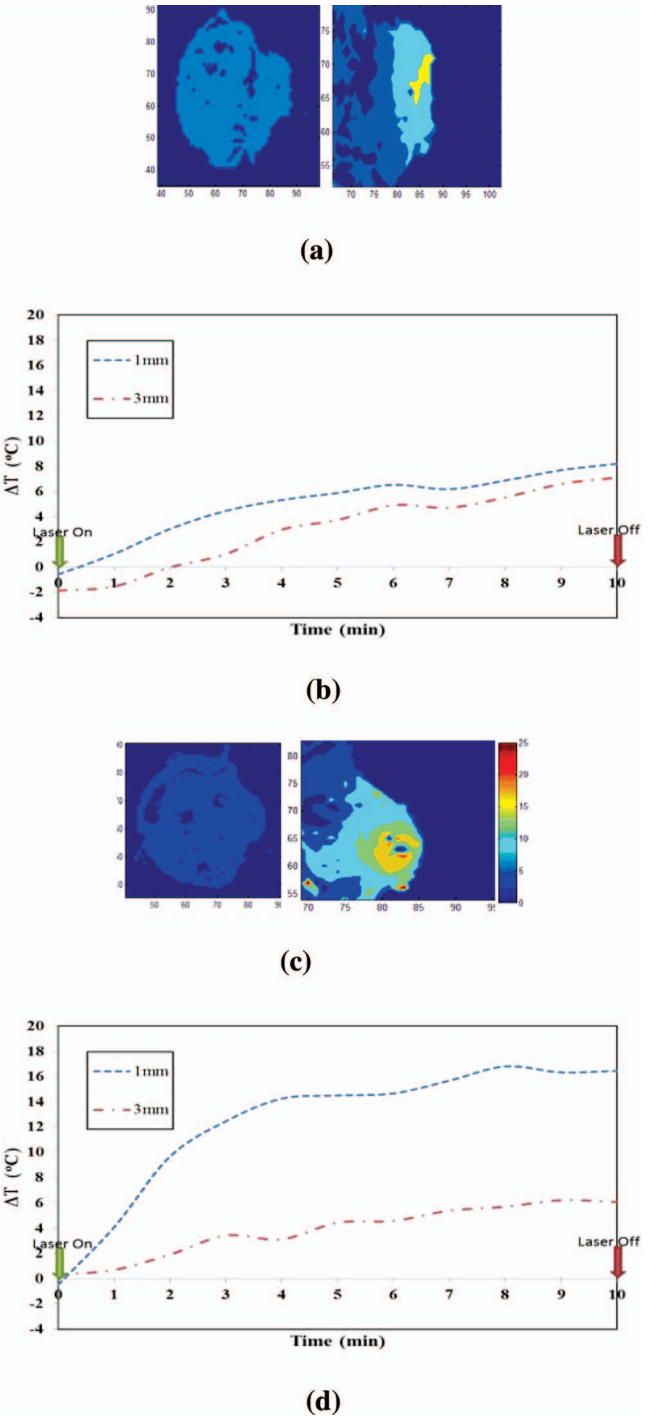

Fig. 6 Rat 1.0 and 1.5 W PRF spatial and temporal assessments. Temperature profiles in a rat during interstitial laser treatment with a power of 1.0 W for 10 min. See Fig. 1(a) for the selection of slices with the 0.5-cm active tip. MR thermographic isoplots of tissue temperature were acquired from the fifth slice, before [(a), left panel] and immediately after [(a), right panel] irradiation. A closer examination (b) shows an increase of 7°C and 8°C at positions of 3 and 1 mm away from the active tip, respectively. These smaller temperature differences correspond to a more even distribution of temperature. Temperature profiles of a rat during interstitial laser treatment with a power of 1.5 W for 10 min. MR thermographic isoplots of tissue temperature were acquired from the fifth slice, before [(c), left panel] and immediately after [(c), right panel] irradiation. A closer examination (d) shows an increase of 8°C and 17°C at positions of 3 and 1 mm away from the active tip, respectively.

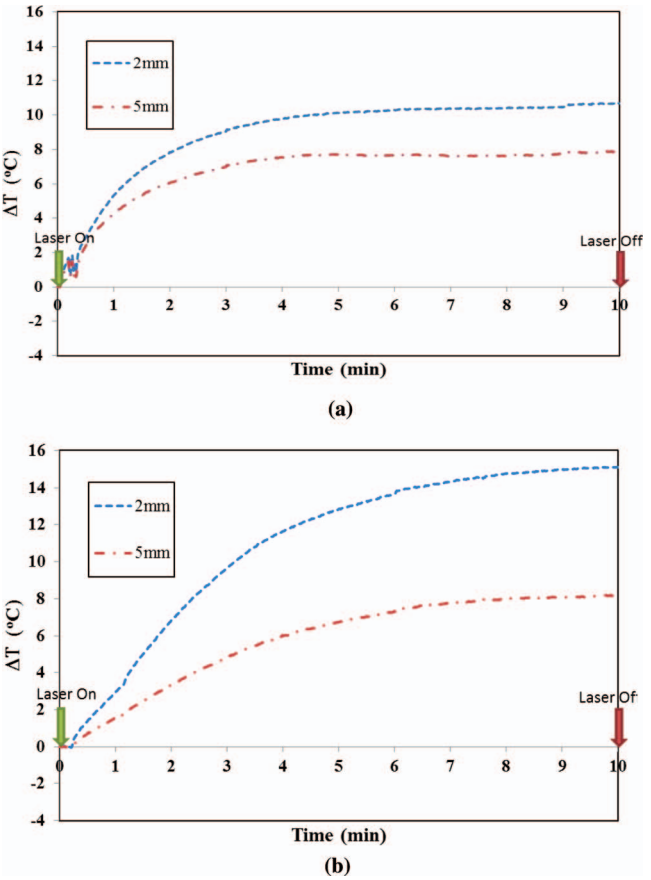

Fig. 7 Rat 1.0 and 1.5 W thermocouple temporal assessments. Temperature increases in a rat tumor during interstitial laser irradiation of 1.0 W (a) and 1.5 W (b) for 10 min measured using thermocouples. The measurement distances are approximately 2 and 5 mm from the active tip. The maximum temperature elevations are 8°C and 11°C for 1.0 W (a) and 8°C and 15°C for 1.5 W (b). These measurements are close to the results obtained using PRF, as shown in Figs. 6(b) and 6(d).

of the temperature reaching a steady state, which may explain the effect seen in Fig. 5.

Variations in tissue compositions not only affected the PRF results, but also the temperature conductance, as shown in Figs. 5 and 6. The thermal resistance was relatively high when 1.5 W was used, as evidenced by a major drop in temperature elevation just 2 mm from the laser source. In these cases, a higher power or longer laser irradiation duration was needed to overcome these physical barriers and to increase the likelihood of temperature saturation. Nevertheless, moderate laser power and irradiation duration may be the best solution in terms of biological and thermal interactions.

Although we ascribed the major anomalies such as temperature fluctuations and distortions from the PRF results to tissue homogeneity and motion artifacts, it is worth noting other potential factors inherent in this modality. According to Maswadi et al., with the increase in laser power and temperature elevation, the signal-to-noise ratio (SNR) decreases as the phase change deviation increases.[45] In terms of temperature resolution, for a temperature increase of 20°C, the resolution in 2D MRT decreases to 1.4°C (calculation based on a 2 T MRT). In the treatment of cancer, temperature elevation above 20°C is not necessary and may be detrimental to a total immune response as discussed earlier. However, with the exception of the liver results and artifact from Fig. 5 at the 5–6 min marks, we can reasonable assume (based on a higher SNR of 7.1 T MRT) that the temperature excursion error contribution is much less than 1.4°C. In addition, as reported by Peters et al., another potential source of error is due to the physical presence of the heat source within the target. In their investigation, there was an orientation-dependent effect on the measured temperature that was attributed to the magnetic susceptibility of tissue along the 1-cm diffuser.[46,47] This is an issue that we will address in future studies.

Tumor size was an important factor affecting temperature increase. Due to a finite spatial resolution, the tumor size cannot be too small for reliable assessment.

Laser immunotherapy using a noninvasive application mode may not be optimal due to the intervening skin. It was also observed that the internal tissue composition had a major effect on photothermal activity. Care must be taken especially when administering treatment to large tumors. Increasing the power by 0.5 W will assure a major temperature increase within a 1-mm radius of the ROI, but not necessarily for a 3-mm radius of a ROI. It is worth noting that ILIT does not need to completely destroy all tumor cells in order to stimulate an effective immune response. Therefore, a balance of laser power and irradiation duration should be considered when determining treatment protocols. Furthermore, a nonuniform temperature distribution in the target tissue may lead to better immunological stimulation since tumor cells injured or disturbed at different levels may provide different immune responses. Control of residual tumors and metastasis after laser immunotherapy may rely on all the components of host immune system. Indeed, further studies are needed to correlate the immunological responses with tissue temperature.

5 Conclusions

Photothermal interactions and immunological reactions are at the heart of LIT. Understanding the photothermal effect is the first step toward a greater understanding of the mechanism of LIT and an improved treatment protocol.

In this study, we investigated photothermal effects during interstitial laser irradiation using PRF. To the best of our knowledge, this is the first time that a 7.1 T MRI has been used to monitor temperature distribution during interstitial laser irradiation in target tissue via PRF. Indeed, this magnetic field strength is much higher than conventional clinical MRIs and currently it may not be particularly relevant to clinical application to humans. However, we believe that, as a first step in proving the feasibility of the PRF method for ILIT applications, it is necessary to begin with a stronger magnet to have better SNR and image resolution.

Understanding the mechanism of metastasis is a big challenge, requiring vast knowledge from many disciplines. Understanding how laser and tissue interact is one of the key factors for a better treatment outcome, particularly in ILIT, since temperature increase is crucial for tumor destruction and antigen release. Parameters such as laser power and irradiation time are crucial for the final outcome.

With PRF, we can assess the photothermal interaction down to the pixel level and make changes as needed. In this study,

the tissue composition was the most crucial factor contributing to variant thermal conductance inside of a tumor. Our results provide some basic understanding needed to control the thermal damage inside a tumor using interstitial laser treatment. Furthermore, our work may lead to an optimal protocol for future cancer treatment using interstitial phototherapy in conjunction with immunotherapy. The development of ILIT may lead to an efficient method to treat various forms of cancer at various stages. With reliable temperature feedback using PRF, a possible correlation between temperature and immunological response could be established for future cancer treatment.

Appendix

```
% MATLAB Code
% 3D unwrapping
% Delta_T is the wrapped image set. The input file
% Delta_X is the unwrapped image set
% need to change these parameter to the specific MRI settings
cycle = 70;
gamma = 2*pi*42.67*10^6;
B = 7.05;
TE = 4×10^-3;
Alpha = -0.01×10^-6;
ConstantD = gamma*B*TE*Alpha;

if unwrap = 1
for x = 1:1
  Delta_X = DeltaT;
  for rep = 1:cycle
    for row = 1:d1
      for col = 1:d2
        if (Delta_X(row,col,rep)< -10)
          Delta_X(row,col,rep) = ( -2*pi/ConstantD) + DeltaT
          (row,col,rep);
          if rep = cycle

          end
        end
      end
    end
  end
end
```

Acknowledgments

This research is supported by grants from the US National Institutes of Health (P20RR016478-10 from the INBRE Program of the National Center for Research Resources) and from ImmunoPhotonics, Inc.

References

1. A. Carpi, A. Nicolini, A. Antonelli, P. Ferrari, and G. Rossi, "Cytokines in the management of high risk or advanced breast cancer: an update and expectation," *Current Cancer Drug Targets* **9**, 888–903 (2009).
2. S. Kim-Schulze, B. Taback, and H. L. Kaufman, "Cytokine therapy for cancer," *Surg. Oncol. Clin. N. Am.* **16**, 793–818 (2007).
3. E. A. Eksioglu, S. Eisen, and V. Reddy, "Dendritic cells as therapeutic agents against cancer," *Front Biosci*. **15**, 321–347 (2010).
4. P. Kalinski, J. Urban, R. Narang, E. Berk, E. Wieckowski, and R. Muthuswamy, "Dendritic cell-based therapeutic cancer vaccines: what we have and what we need," *Future Oncology* **5**, 379–390 (2009).
5. H. G. Zhang, K. Mehta, P. Cohen, and C. Guha, "Hyperthermia on immune regulation: a temperature's story," *Cancer Lett.* **271**, 191–204 (2008).
6. A. P. Castano, P. Mroz, and M. R. Hamblin, "Photodynamic therapy and anti-tumour immunity," *Nat. Rev. Cancer* **6**, 535–545 (2006).
7. J. Begley and A. Ribas, "Targeted therapies to improve tumor immunotherapy," *Clin. Cancer Res.* **14**, 4385–4391 (2008).
8. W. R. Chen, R. L. Adams, R. Carubelli, and R. E. Nordquist, "Laser-photosensitizer assisted immunotherapy: A novel modality in cancer treatment," *Cancer Lett.* **115**, 25–30 (1997).
9. W. R. Chen, W.-G. Zhu, J. R. Dynlacht, H. Liu, and R. E. Nordquist, "Long-term tumor resistance induced by laser photo-immunotherapy," *Int. J. Cancer* **81**, 808–812 (1999).
10. W. R. Chen, H. Liu, J. A. Nordquist, and R. E. Nordquist, "Tumor cell damage and leukocyte infiltration after laser immunotherapy treatment," *Lasers Med. Sci.* **15**, 43–48 (2000).
11. W. R. Chen, A. K. Singhal, H. Liu, and R. E. Nordquist, "Antitumor immunity induced by laser immunotherapy and its adoptive transfer," *Cancer Res.* **61**, 459–461 (2001).
12. W. R. Chen, H. Liu, J. W. Ritchey, K. E. Bartels, M. D. Lucroy, and R. E. Nordquist, "Effect of different components of laser immunotherapy in treatment of metastatic tumors in rats," *Cancer Res.* **62**, 4295–4299 (2002).
13. W. R. Chen, S. W. Jeong, M. D. Lucroy, R. F. Wolf, E. W. Howard, H. Liu, and R. E. Nordquist, "Induced anti-tumor immunity against DMBA-4 metastatic mammary tumors in rats using a novel approach," *Int. J. Cancer* **107**, 1053–1057 (2003).
14. M. F. Naylor, W. R. Chen, T. K. Teague, L. Perry, and R. E. Nordquist, "*In situ* photo immunotherapy: a tumor-directed treatment modality for melanoma," *Br. J. Dermatol.* **155**, 1287–1292 (2006).
15. X. Li, M. F. Naylor, R. E. Nordquist, T. K. Teague, C. A. Howard, C. Murray, and W. R. Chen, "*In situ* photoimmunotherapy for late-stage melanoma patients: a preliminary study," *Cancer Biology and Therapy* **10**(11), 1081–1087 (2010).
16. X. Li, G. L. Ferrel, M. C. Guerra, T. Hode, J. A. Lunn, O. Adalsteinsson, R. E. Nordquist, H. Liu, and W. R. Chen, "Preliminary safety and efficacy results of laser immunotherapy for the treatment of metastatic breast cancer patients," *Photochem. Photobiol. Sci.* **10**, 817–821 (2011).
17. W. R. Chen, R. L. Adams, S. Heaton, D. T. Dickey, K. E. Bartels, and R. E. Nordquist, "Chromophore-enhanced laser-tumor tissue photothermal interaction using 808 nm diode laser," *Cancer Lett.* **88**, 15–19 (1995).
18. W. R. Chen, R. L. Adams, K. E. Bartels, and R. E. Nordquist, "Chromophore-enhanced *in vivo* tumor cell destruction using an 808-nm diode laser," *Cancer Lett.* **94**, 125–131 (1995).
19. W. R. Chen, R. L. Adams, A. K. Higgins, K. E. Bartels, and R. E. Nordquist, "Photothermal effects on murine mammary tumors using indocyanine green and an 808-nm diode laser: An *in vivo* efficacy study," *Cancer Lett.* **98**, 169–173 (1996).
20. M. H. den Brok, R. P. Sutmuller, R. van der Voort, E. J. Bennink, C. G. Figdor, T. J. Ruers, and G. J. Adema, "In situ tumor ablation creates an antigen source for the generation of antitumor immunity," *Cancer Res.* **64**, 4024–4029 (2004).
21. X. Li, F. Zhou, H. Le, R. F. Wolf, E. Howard, R. E. Nordquist, T. Hode, H. Liu, and W. R. Chen, "Mechanism study of tumor-specific immune responses induced by laser immunotherapy," *Proc. SPIE* **7900**, 790006 (2011).
22. S. Thompson, A. C. Self, and C. H. Self, "Light-activated antibodies in the fight against primary and metastatic cancer," *Drug Discovery Today* **15**(11–12), 468–473 (2010).
23. E. Jager, D. Jager, and A. Knuth, "Antigen-specific immunotherapy and cancer vaccines," *Int. J. Cancer* **106**, 820–917 (2003).
24. M. H. den Brok, R. P. Sutmuller, S. Nierkens, E. J. Bennink, C. Frielink, L. W. J. Toonen, O. C. Boerman, C. G. Figdor, T. J. Ruers, and G. J. Adema, "Efficient loading of dendritic cells following cryo and radiofrequency ablation in combination with immune modulation induces anti-tumour immunity," *Br. J. Cancer* **95**, 896–905 (2006).
25. A. Mukhopadhaya, J. Mendecki, X. Dong, L. Liu, S. Kalnicki, M. Garg, A. Alfieri, and C. Guha, "Localized hyperthermia combined with intratumoral dendritic cells induces systemic antitumor immunity," *Cancer Res.* **67**, 7798–7806 (2007).

26. T. Chen, J. Guo, C. Han, M. Yang, and X. Cao, "Heat shock protein 70, released from heat-stressed tumor cells, initiates antitumor immunity by inducing tumor cell chemokine production and activating dendritic cells via TLR4 pathway," *J. Immunol.* **182**, 1449–1459 (2009).
27. M. N. Rylander, Y. Feng, J. Bass, and K. R. Diller, "Heat shock protein expression and injury optimization for laser therapy design," *Lasers Surg. Med.* **39**, 731–746 (2007).
28. R. Lovell, L. Madden, L. R. McNaughton, and S. Carroll, "Effects of active and passive hyperthermia on heat shock protein 70 (HSP70)," *Amino Acids* **34**, 203–211 (2008).
29. M. Horowitz and S. D. Robinson, "Heat shock proteins and the heat shock response during hyperthermia and its modulation by altered physiological conditions," *Prog. Brain Res.* **162**, 433–446 (2007).
30. K. Kuroda, "Non-invasive MR thermography using the water proton chemical shift," *Int. J. Hyperthermia* **21**(6), 547–560 (2005).
31. J. De Poorter, C. de Wagter, Y. de Deene, C. Thomsen, F. Stahlberg, and E. Achten, "Noninvasive MRI thermometry with the proton resonance frequency (PRF) method: *in vivo* results in human muscle," *Magn. Reson. Med.* **33**, 74–81 (1995).
32. Q. Bruno, J. A. de Zwart, and C. T. Woonen, "Magnetic resonance temperature imaging for guidance of thermotherapy," *J. Magn. Reson. Imaging* **12**, 525–533 (2000).
33. J. C. Hindman, "Proton resonance shift of water in the gas and liquid states," *J. Chem. Phys.* **44**(12), 4582–4592 (1996).
34. K. Kuroda, "Temperature mapping using the water proton chemical shift: a chemical shift selective phase mapping method," *Magn. Reson. Med.* **38**(5), 845–851 (1997).
35. R. Stollberger, P. W. Ascher, D. Huber, W. Renhart, H. Radner, and F. Ebner, "Temperature monitoring of interstitial thermal tissue coagulation using MR phase images," *J. Magn. Reson. Imaging* **8**, 188–196 (1998).
36. J. Olsrud, R. Wirestam, S. Brockstedt, A. M. Nilsson, K.-G. Tranberg, F. Stahlberg, and B. R. R. Persson, "MRI thermometry in phantoms by use of the proton resonance frequency shift method: application to interstitial laser thermotherapy," *Phys. Med. Biol.* **43**, 2597–2613 (1998).
37. Y. Ishihara, A. Calderon, H. Wantanabe, K. Okamoto, Y. Suzuki, K. Kuroda, and Y. Suzuki, "A precise and fast temperature mapping using water proton chemical shift," *Magn. Reson. Med.* **34**(6), 814–823 (1995).
38. S. C. Gnyawali, Y. Chen, F. Wu, K. E. Bartels, J. P. Wicksted, H. Liu, and W. R. Chen, "Temperature measurement on tissue surface during laser irradiation," *Med. Biol. Eng. Comput.* **46**, 159–168 (2008).
39. Y. Chen, S. C. Gnyawali, F. Wu, H. Liu, Y. A. Tesiram, A. Abbott, R. A. Towner, and W. R. Chen, "Magnetic resonance imaging guidance for laser photothermal therapy," *J. Biomed. Opt.* **13**, 044033 (2008).
40. T. Kahn, T. Harth, J. C. Kiwit, H. J. Schwarzmaier, C. Wald, and U. Mödder, "*In vivo* MRI thermometry using a phase-sensitive sequence: Preliminary experience during MRI-guided laser induced interstitial thermotherapy of brain tumors," *J. Magn. Reson. Imaging* **8**, 160–164 (1998).
41. J. Depoorter, C. Dewagter, Y. Dedeene, C. Thomsen, F. Stahlberg, and E. Achten, "The proton-resonance-frequency-shift method compared with molecular diffusion for quantitative measurement of two-dimensional time-dependent temperature distribution in a phantom," *J. Magn. Reson. Ser B* **103**(3), 234–241 (1994).
42. Y. Chung, J. L. Duerk, A. Shankaranarayanan, M. Hampke, E. M. Merkle, and J. S. Lewin, "Temperature measurement using echo-shifted FLASH at low field for interventional MRI," *J. Magn. Reson. Imaging* **9**(1), 138–145 (1999).
43. S. Grimault, T. Lucas, S. Quellec, and F. Mariette, "Quantitative measurement of temperature by proton resonance frequency shift at low field: a general method to correct non-linear spatial and temporal phase deformations," *J. Magn. Reson.* **170**(1), 79–87 (2004).
44. K. J. Barkauskas, J. S. Lewin, and J. L. Duerk, "Variation correction algorithm: analysis of phase suppression and thermal profile fidelity for proton resonance frequency magnetic resonance thermometry at 0.2 T," *J. Magn. Reson. Imaging* **17**(2), 227–240 (2003).
45. S. M. Maswadi, R. D. Glickman, S. J. Dodd, and J. Gao, "Temperature mapping of laser-induced hyperthermia in an ocular phantom using magnetic resonance thermography," *J. Biomed. Opt*, **9**, 711–718 (2004).
46. R. D. Peters, R. S. Hinks, and R. M. Henkelman, "Heat-source orientation and geometry dependence in proton-resonance frequency shift magnetic resonance thermometry," *Magn. Reson. Med.* **41**(5), 909–918 (1999).
47. J. C. Chen, J. A. Moriarty, J. A. Derbyshire, R. D. Peters, J. Trachtenberg, S. D. Bell, J. Doyle, R. Arrelano, G. A. Wright, R. M. Henkelman, R. S. Hinks, S. Y. Lok, A. Toi, and W. Kucharczyk, "Prostate cancer: MR imaging and thermometry during microwave thermal ablation-initial experience," *Radiology* **214**(1), 290–297 (2000).